Available online at www.sciencedirect.com
SCIENCE DIRECT®
International Journal of Thermal Sciences 45 (2006) 378–389
International Journal of Thermal Sciences
www.elsevier.com/locate/ijts

The Falkner–Skan flow with constant wall temperature and variable viscosity

A. Pantokratoras

School of Engineering, Democritus University of Thrace, 67100 Xanthi, Greece

Received 27 January 2005; received in revised form 9 June 2005; accepted 9 June 2005
Available online 1 August 2005

Abstract

A theoretical study of the effect of variable viscosity on the classical Falkner–Skan flow is presented in this paper. The results are obtained with the direct numerical solution of the boundary layer equations. Velocity and temperature profiles are shown graphically and wall heat transfer and wall shear stress are listed in tables for Prandtl numbers from 1 to 10 000. The effect of different parameters on the flow field is discussed.

Keywords: Temperature-dependent viscosity; Falkner–Skan flow; Forced convection

1. Introduction

The fluid flow along a stationary plate is a classical problem of fluid mechanics known as the Blasius problem. In this case the free stream is parallel to the plate and its velocity is constant. If the wall makes a positive angle with the free stream, then the free stream is accelerated along the wall and we have the Falkner–Skan flow along a wedge. Falkner and Skan [1] showed that this problem admits similarity solution as happens with the Blasius problem. Hartree [2] solved this problem and gave numerical results for the wall shear stress for different values of the wedge angle. These values can be found in fluid mechanics textbooks (see for example Bejan [3]). The heat transfer similarity solution can be developed in the same way by substituting the Falkner–Skan similarity momentum equation into the boundary layer energy equation. Eckert [4] solved the Falkner–Skan flow along an isothermal wedge and gave the first wall heat transfer values. Thereafter, many solutions have been obtained for different aspects of this class of boundary layer problems. Lin and Lin [5] provided very accurate solutions for wall heat transfer from either an isothermal or uniform flux wedge to fluids for any Prandtl number.

When the fluid is assumed to have constant properties then the problem is uncoupled, that is, the momentum equation has an influence on the energy equation but the energy equation has not any influence on the momentum equation. However, most fluids have temperature-dependent viscosity and this property varies significantly when large temperature differences exist. In this case the two equations are coupled and each equation affects the other. The first attempt to solve the Falkner–Skan problem including the variation of viscosity with temperature was made by Herwing and Wickern [6] who used an asymptotic expansion method valid only for small heat transfer rates. Hossain et al. [7] studied the flow of a fluid with temperature dependent viscosity past a permeable wedge with uniform surface heat flux. In another paper Hossain et al. [8] extended the previous work considering both viscosity and thermal conductivity as functions of temperature. The above two works concern uniform heat flux at the surface while the Prandtl number has been assumed constant across the boundary layer. Elbashbeshy and Dimian [9] investigated the effect of variable viscosity and radiation on flow and heat transfer over a wedge with constant surface temperature but only for $m = 1/3$ and assuming

E-mail address: apantokr@civil.duth.gr (A. Pantokratoras).

1290-0729/$ – see front matter
doi:10.1016/j.ijthermalsci.2005.06.004

again that the Prandtl number is constant inside the boundary layer. The objective of the present paper is to present results for the classical Falkner–Skan problem with constant surface temperature considering both viscosity and Prandtl number variable across the boundary layer and covering a wide range of Prandtl numbers and exponents m. The results are obtained with the direct numerical solution of the boundary layer equations. A direct solution procedure of the untransformed equations has been also used by Nanbu [10] for the unsteady Falkner–Skan problem with constant properties.

2. The mathematical model

Consider the flow along a wedge placed in a flowing fluid with u and v denoting respectively the velocity components in the x and y direction, where x is the coordinate along the wedge surface and y is the coordinate perpendicular to x (see Fig. 1). For steady, two-dimensional flow the boundary layer equations including variable viscosity are

- continuity equation:

$$\frac{\partial u}{\partial x}+\frac{\partial v}{\partial y}=0 \tag{1}$$

- momentum equation:

$$u\frac{\partial u}{\partial x}+v\frac{\partial v}{\partial y}=\frac{1}{\rho_a}\frac{\partial}{\partial y}\left(\mu\frac{\partial u}{\partial y}\right)+u_a\frac{\partial u_a}{\partial x} \tag{2}$$

- energy equation:

$$u\frac{\partial T}{\partial x}+v\frac{\partial T}{\partial y}=\alpha\frac{\partial^2 T}{\partial y^2} \tag{3}$$

where T is the fluid temperature, μ is the dynamic viscosity, α is the thermal diffusivity, and ρ_a is the ambient fluid density.

The boundary conditions are as follows:

$$\text{at } y=0, \quad u=0, \quad v=0, \quad T=T_w \tag{4}$$

$$\text{as } y\to\infty, \quad u_a=u_0x^m, \quad T=T_a \tag{5}$$

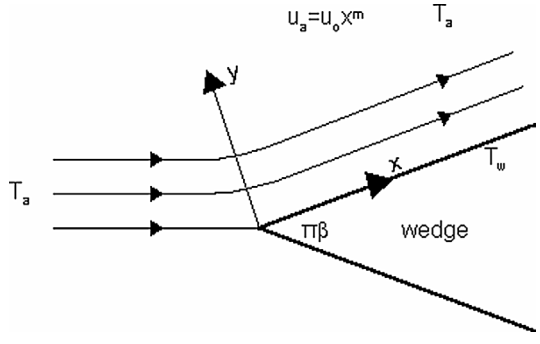

Fig. 1. The flow configuration and coordinate system.

where T_w is the wedge temperature, T_a is the ambient fluid temperature, u_a is the free stream velocity and u_0 is a constant. The exponent m, which is called the Falkner–Skan power-law parameter, is related to the wedge angle β by $m=\beta/(2-\beta)$.

The viscosity is assumed to be an inverse linear function of temperature given by the following equation [11]

$$\frac{1}{\mu}=\frac{1}{\mu_a}\left[1+\gamma(T-T_a)\right] \tag{6}$$

where μ_a is the ambient fluid dynamic viscosity and γ is a thermal property of the fluid. Eq. (6) can be rewritten a follows

$$\frac{1}{\mu}=a(T-T_r) \tag{7}$$

where $a=\gamma/\mu_a$ and $T_r=T_a-1/\gamma$ are constants and their values depend on the reference state and the thermal property of the fluid.

Eqs. (1), (2) and (3) represent a two-dimensional parabolic flow. Such a flow has a predominant velocity in the streamwise coordinate which in our case is the direction along the wedge surface. The equations were solved directly, without any transformation, using the finite difference method of Patankar [12]. In the numerical solution of the boundary layer problems the calculation domain must always be at least equal or wider than the boundary layer thickness. However, it is known that the boundary layer thickness increases with x. If a Cartesian grid, formed by lines of constant x and y is chosen, the number of grid points within the boundary layer for small values of x, where the boundary layer is thin, is small and the computational accuracy is low. If the mesh length is reduced to have more points in the boundary layer at small x, the grid points at large x becomes excessive. Therefore, it would be desirable to have a grid which conforms to the actual shape of the boundary layer. In this work an expanding grid has been used according to the following equation

$$y_{out}=y_0+cx \tag{8}$$

where y_{out} is the outer boundary, c is the spreading rate of the outer boundary and x is the distance at the current step. The forward step size Δx increases in proportion to the width of the calculation domain and was 1% of the outer boundary. In order to obtain a complete form of both the temperature and velocity profile at the same cross section we used a nonuniform lateral grid. Δy takes small values near the wedge (many grid points near the wedge) and increases along y. The lateral grid cells were 500.

The solution procedure starts with a known distribution of velocity and temperature at the wedge edge ($x=0$) and marches along the wedge. Flat velocity and temperature profiles were assumed at the wedge edge. These profiles were used only to start the computations and their shape had no influence on the results which were taken far downstream (see Fig. 2). At each downstream position the discretized

equations (2) and (3) are solved using the tridiagonal matrix algorithm (TDMA). The cross-stream velocities v were obtained from the continuity equation. As x increases the successive velocity profiles become more and more similar and the same happens with temperature profiles. The solution procedure stops at the point where the successive velocity and temperature profiles become identical. The results are grid independent. The parabolic solution procedure is a well known solution method and has been used extensively in the literature. It appeared for the first time in 1970 [13] and has been included in classical fluid mechanics textbooks (see page 275 in White [14]). A detailed description of the solution procedure, with variable thermophysical properties, may be found in Pantokratoras [15]. In the vicinity of the leading edge the problem is elliptic and the present parabolic procedure is not valid. However, as x increases the elliptic effects decay rapidly and the problem turns from elliptic to parabolic. We used the above parabolic procedure in the entire region taking into account that we are interested in results at long distances from the leading edge were the problem is purely parabolic.

The coincidence of successive velocity and successive temperature profiles at large x is a proof that the present problem admits similarity solution. This means that the present problem could be treated with the classical similarity method used for variable viscosity problems (see for example Pop et al. [16]). In the classical similarity method the transformed energy equation contains the Prandtl number, which is usually treated as a constant across the boundary layer. However, the Prandtl number is a function of viscosity and as viscosity varies across the boundary layer, the Prandtl number varies, too. The assumption of constant Prandtl number in the classical similarity method leads to unrealistic results when viscosity is a strong function of temperature [17]. For that reason we used the direct solution procedure of Patankar which gives accurate results even for strong relationship between viscosity and temperature.

3. Results and discussion

The most important quantities for this problem are the wall heat transfer and the wall shear stress defined as [16]

$$\theta'(0) = -\frac{x}{T_\mathrm{w} - T_\mathrm{a}}\, Re^{-1/2} \left[\frac{\partial T}{\partial y}\right]_{y=0} \tag{9}$$

$$f''(0) = \frac{\vartheta_\mathrm{r} - 1}{\vartheta_\mathrm{r}} \frac{\mu_\mathrm{w}}{\rho_\mathrm{a} u_\mathrm{a}^2}\, Re^{1/2} \left[\frac{\partial u}{\partial y}\right]_{y=0} \tag{10}$$

where θ is the dimensionless temperature $(T - T_\mathrm{a})/(T_\mathrm{w} - T_\mathrm{a})$, μ_w is the fluid viscosity at the wedge surface and f is the dimensionless stream function for which the following equation is valid

$$f' = \frac{u}{u_\mathrm{a}} \tag{11}$$

The Reynolds number is defined as

$$Re = \frac{u_\mathrm{a} x}{\nu_\mathrm{a}} \tag{12}$$

and θ_r is a constant defined by

$$\theta_\mathrm{r} = \frac{T_\mathrm{r} - T_\mathrm{a}}{T_\mathrm{w} - T_\mathrm{a}} = -\frac{1}{\gamma (T_\mathrm{w} - T_\mathrm{a})} \tag{13}$$

In Eqs. (9), (10) and (11) the prime represents differentiation with respect to similarity variable η defined as

$$\eta = \frac{y}{x}\, Re^{1/2} \tag{14}$$

When the wedge temperature is greater than the ambient one (fluid heating), negative θ_r corresponds to liquids and positive θ_r to gases. The opposite happens for fluid cooling. In this case negative θ_r corresponds to gases and positive θ_r to liquids. It should be mentioned here that when $\theta_\mathrm{r} \to \infty$ the fluid viscosity becomes equal to ambient viscosity, that is, viscosity is constant inside the boundary layer and we have the classical Falkner–Skan flow where the momentum equation is not affected by the energy equation. When the relationship between viscosity and temperature is strong (large γ) or the temperature difference between the plate and the ambient fluid is large, then $\theta_\mathrm{r} \to 0$.

In order to test the accuracy of the present method, results were compared with those available in the literature. First we checked the influence of the boundary conditions at $x = 0$ on the results. If we assume that $m = 0$ and θ_r is infinite then we have the classical Blasius problem with constant viscosity. The wall shear stress of the Blasius problem is given by the following equation [14, p. 235]

$$\tau_\mathrm{w} = \frac{0.4696 \mu u_0}{\sqrt{2\nu x / u_0}} \tag{15}$$

where ν is the fluid kinematic viscosity. In Fig. 2 we present the variation of dimensional wall shear stress along the plate for the Blasius problem with free stream velocity $u_0 = 1\ \mathrm{cm{\cdot}sec^{-1}}$, $\mu = 0.05\ \mathrm{gr{\cdot}cm{\cdot}sec^{-1}}$ and $\nu = 0.05\ \mathrm{cm^2{\cdot}sec^{-1}}$. The dashed line has been produced using Eq. (15) and the solid line by the present method solving the boundary layer equations using the above described solution procedure of Patankar [12]. We see that, except for a small region near the plate leading edge, the two methods give identical results. The results of the present work have been taken at large x and this means that our initial profiles at $x = 0$ had no influence on the results.

Figs. 3 and 4 show the velocity and temperature distribution across the boundary layer for ambient Prandtl number 1, $m = 1$ and different values of the viscosity parameter θ_r. The dashed line in Fig. 3 is the similarity solution with constant viscosity (see page 246 in White [14]) and the dashed line in Fig. 4 is the temperature similarity profile with constant viscosity [4]. We see that as the absolute value of the viscosity parameter increases, that is, as viscosity tends to become constant inside the boundary layer, our profiles tend to coincide with the similarity profiles known in the literature. Our

Table 1
Values of $f''(0)$ and $\theta'(0)$ for $Pr_a = 1$

θ_r	$m=-0.05$		$m=0$		$m=1/11$		$m=1/5$		Pr_w
	$f''(0)$	$\theta'(0)$	$f''(0)$	$\theta'(0)$	$f''(0)$	$\theta'(0)$	$f''(0)$	$\theta'(0)$	
∞	0.2135 Harris et al.	0.2994 Harris et al.	0.3320 Hartree	0.3320 Eckert	0.4837 Harris et al.	0.3707 Harris et al.	0.6213 Harris et al.	0.4053 Harris et al.	1.00
−10	0.2320	0.3046	0.3612	0.3410	0.5167	0.3762	0.6619	0.4115	0.91
−8	0.2365	0.3059	0.3672	0.3418	0.5248	0.3776	0.6716	0.4123	0.89
−6	0.2438	0.3079	0.3771	0.3440	0.5376	0.3792	0.6876	0.4146	0.86
−4	0.2582	0.3116	0.3950	0.3463	0.5629	0.3831	0.7186	0.4182	0.80
−2	0.2983	0.3221	0.4491	0.3578	0.6328	0.3926	0.8043	0.4277	0.67
−1	0.3673	0.3380	0.5400	0.3732	0.7275	0.4076	0.9511	0.4423	0.50
−0.1	0.8749	0.4193	1.2582	0.4518	1.7591	0.4832	2.2198	0.5174	0.09
−0.01	2.3211	0.4945	3.4970	0.5198	5.0267	0.5476	6.4149	0.5787	0.01
−0.001	6.8795	0.5303	10.6615	0.5521	15.4823	0.5753	19.8426	0.6053	0.001
2	0.1098	0.2637	0.1909	0.3025	0.2864	0.3371	0.3756	0.3715	2.00
4	0.1642	0.2838	0.2688	0.3221	0.3930	0.3572	0.5090	0.3917	1.33
6	0.1812	0.2895	0.2917	0.3260	0.4248	0.3616	0.5485	0.3968	1.20
8	0.1895	0.2921	0.3038	0.3290	0.4401	0.3644	0.5674	0.3991	1.14
10	0.1944	0.2936	0.3107	0.3315	0.4492	0.3662	0.5785	0.4008	1.11
∞	0.2135	0.2994	0.3320	0.3320	0.4837	0.3707	0.6213	0.4053	1.00

θ_r	$m=1/3$		$m=1$		$m=2$		Pr_w
	$f''(0)$	$\theta'(0)$	$f''(0)$	$\theta'(0)$	$f''(0)$	$\theta'(0)$	
∞	0.7574 Harris et al.	0.4401 Harris et al.	1.2326 Harris et al.	0.5705 Harris et al.	1.7151 Harris et al.	0.7161 Harris et al.	1.00
−10	0.8054	0.4461	1.3070	0.5766	1.8168	0.7235	0.91
−8	0.8170	0.4472	1.3250	0.5780	1.8411	0.7252	0.89
−6	0.8360	0.4490	1.3543	0.5803	1.8812	0.7278	0.86
−4	0.8726	0.4527	1.4111	0.5845	1.9588	0.7328	0.80
−2	0.9742	0.4623	1.5684	0.5957	2.1736	0.7461	0.67
−1	1.1482	0.4777	1.8386	0.6128	2.5391	0.7662	0.50
−0.1	2.6778	0.5535	4.2850	0.6971	5.9075	0.8643	0.09
−0.01	7.7897	0.6133	12.5950	0.7598	17.5025	0.9383	0.01
−0.001	24.1600	0.6391	39.1660	0.7854	54.5402	0.9637	0.001
2	0.4638	0.4051	0.7728	0.5280	1.0849	0.6653	2.00
4	0.6238	0.4257	1.0246	0.5527	1.4308	0.6952	1.33
6	0.6708	0.4311	1.0979	0.5593	1.5308	0.7029	1.20
8	0.6934	0.4340	1.1330	0.5623	1.5789	0.7065	1.14
10	0.7066	0.4351	1.1536	0.5640	1.6070	0.7086	1.11
∞	0.7574	0.4401	1.2326	0.5705	1.7151	0.7161	1.00

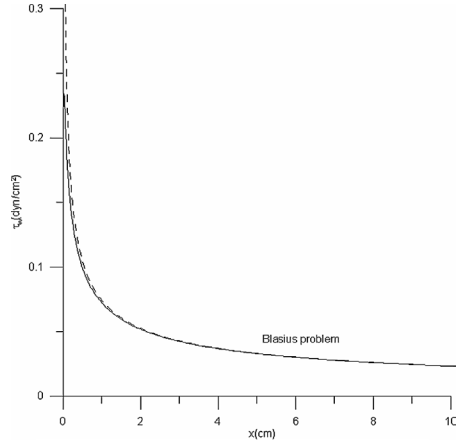

Fig. 2. Variation of wall shear stress for the Blasius problem with free stream velocity 1 cm·sec^{-1}, $\mu = 0.05$ gr·cm·sec^{-1} and $\nu = 0.05$ cm^2·sec^{-1}: dashed line, Blasius solution: solid line, present work.

results with very large θ_r ($\theta_r \to \infty$) coincide completely with the similarity profiles and for that reason are not shown on the figures. The results shown in Figs. 3 and 4 are a second evidence of the accuracy of the present solution procedure.

A third evidence for the accuracy of the present method is the fact that the nondimensional wall shear stress $f''(0)$ and wall heat transfer $\theta'(0)$ calculated from the present method for a fluid with constant viscosity ($\theta_r \to \infty$) coincide with those of Hartree [2], Eckert [4] and Harris et al. [18] as it is seen in the following tables.

In Tables 1–4 and 5 the wall shear stress and the wall heat transfer are given for ambient Prandtl numbers 1, 10, 100, 1000 and 10 000, respectively, and $m = -0.05, 0, 1/11, 1/5, 1/3, 1$ and 2 (these values of m have been used by Harris et al. for the unsteady, constant viscosity Falkner–Skan flow). The correspondence between the exponent m and the wedge angle is as follows:

Table 2
Values of $f''(0)$ and $\theta'(0)$ for $Pr_a = 10$

θ_r	$m=-0.05$		$m=0$		$m=1/11$		$m=1/5$		Pr_w
	$f''(0)$	$\theta'(0)$	$f''(0)$	$\theta'(0)$	$f''(0)$	$\theta'(0)$	$f''(0)$	$\theta'(0)$	
∞	0.2135	0.6380	0.3320 Hartree	0.7281 Eckert	0.4837	0.8325	0.6213	0.9221 Harris et al.	10.00
−10	0.2356	0.6527	0.3669	0.7380	0.5235	0.8480	0.6704	0.9378	9.10
−8	0.2410	0.6562	0.3741	0.7425	0.5332	0.8518	0.6284	0.9418	8.89
−6	0.2500	0.6621	0.3844	0.7473	0.5493	0.8576	0.7021	0.9480	8.57
−4	0.2680	0.6733	0.4106	0.7585	0.5809	0.8692	0.7407	0.9600	8.00
−2	0.3207	0.7041	0.4775	0.7903	0.6710	0.9005	0.8503	0.9931	6.67
−1	0.4205	0.7552	0.6082	0.8415	0.8336	0.9518	1.0457	1.0460	5.00
−0.1	1.3483	1.0563	1.7175	1.1326	2.1975	1.2391	2.6602	1.3376	0.91
−0.01	2.7670	1.3188	3.9054	1.4042	5.4155	1.5174	6.8083	1.6246	0.10
−0.001	7.3100	1.5624	11.0065	1.6318	15.8117	1.7322	20.1967	1.8284	0.01
2	0.1027	0.5469	0.1766	0.6302	0.2642	0.7341	0.3464	0.8168	20.00
4	0.1583	0.5966	0.2586	0.6822	0.3785	0.7888	0.4908	0.8747	13.33
6	0.1769	0.6111	0.2848	0.6967	0.4145	0.8042	0.5357	0.8917	12.00
8	0.1861	0.6182	0.2984	0.7032	0.4322	0.8117	0.5576	0.8993	11.43
10	0.1917	0.6223	0.3059	0.7078	0.4426	0.8162	0.5706	0.9041	11.11
∞	0.2135	0.6380	0.3320	0.7281	0.4837	0.8325	0.6213	0.9221	10.00

θ_r	$m=1/3$		$m=1$		$m=2$		Pr_w
	$f''(0)$	$\theta'(0)$	$f''(0)$	$\theta'(0)$	$f''(0)$	$\theta'(0)$	
∞	0.7574 Hartree	1.0115 Eckert	1.2326 Hartree	1.3388 Eckert	1.7151	1.6977	10.00
−10	0.8155	1.0284	1.3219	1.3601	1.8364	1.7231	9.10
−8	0.8296	1.0327	1.3437	1.3648	1.8659	1.7295	8.89
−6	0.8529	1.0393	1.3794	1.3728	1.9143	1.7392	8.57
−4	0.8984	1.0522	1.4490	1.3885	2.0084	1.7583	8.00
−2	1.0271	1.0861	1.6442	1.4297	2.2720	1.8082	6.67
−1	1.2548	1.1415	1.9853	1.4958	2.7291	1.8906	5.00
−0.1	3.1258	1.4417	4.7913	1.8473	6.5148	2.3121	0.91
−0.01	8.1965	1.7391	13.0650	2.1937	18.0205	2.7206	0.10
−0.001	24.5381	1.9386	39.6522	2.4033	54.6120	2.9576	0.01
2	0.4279	0.9002	0.7138	1.2005	1.0042	1.5272	20.00
4	0.6018	0.9624	0.9900	1.2782	1.3841	1.6233	13.33
6	0.6555	0.9801	1.0742	1.3000	1.4995	1.6500	12.00
8	0.6816	0.9882	1.1150	1.3104	1.5548	1.6627	11.43
10	0.6971	0.9932	1.1391	1.3164	1.5878	1.6700	11.11
∞	0.7574	1.0115	1.2326	1.3388	1.7151	1.6977	10.00

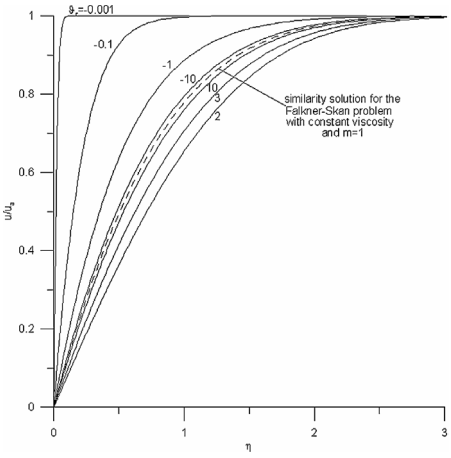

Fig. 3. Velocity distribution for ambient Prandtl number 1, $m = 1$ and different values of the viscosity parameter θ_r. Solid lines correspond to variable viscosity and dashed line to similarity solution with constant viscosity.

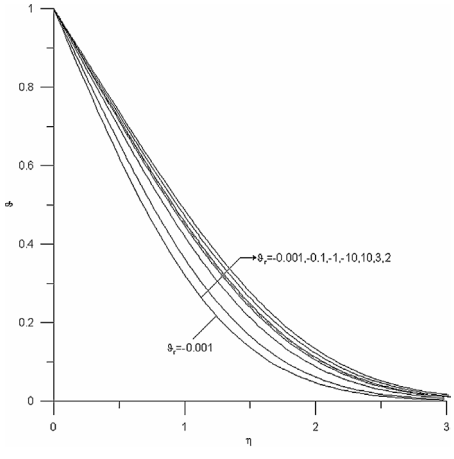

Fig. 4. Temperature distribution for ambient Prandtl number 1, $m = 1$ and different values of the viscosity parameter θ_r. Solid lines correspond to variable viscosity and dashed line to similarity solution with constant viscosity.

Table 3
Values of $f''(0)$ and $\theta'(0)$ for $Pr_a = 100$

θ_r	$m=-0.05$		$m=0$		$m=1/11$		$m=1/5$		Pr_w
	$f''(0)$	$\theta'(0)$	$f''(0)$	$\theta'(0)$	$f''(0)$	$\theta'(0)$	$f''(0)$	$\theta'(0)$	
∞	0.2135	1.3555	0.3320	1.5719	0.4837	1.8152	0.6213	2.0236	100
			Hartree						
−10	0.2363	1.3882	0.3654	1.6032	0.5281	1.8543	0.6771	2.0660	91
−8	0.2419	1.3967	0.3734	1.6122	0.5392	1.8640	0.6910	2.0765	89
−6	0.2514	1.4098	0.3867	1.6255	0.5575	1.8794	0.7137	2.0931	86
−4	0.2702	1.4355	0.4133	1.6542	0.5938	1.9094	0.7589	2.1252	80
−2	0.3270	1.5082	0.4922	1.7301	0.7006	1.9928	0.8909	2.2144	67
−1	0.4403	1.6345	0.6459	1.8615	0.9045	2.1344	1.1406	2.3662	50
−0.1	2.0861	2.6052	2.6054	2.8303	3.2582	3.1228	3.8620	3.3893	9
−0.01	5.5075	3.5757	6.3990	3.7605	7.6622	4.0392	8.9555	4.3176	1
−0.001	8.7143	4.1713	12.3260	4.4425	17.0822	4.8005	21.4537	5.1368	0.1
2	0.1030	1.1556	0.1687	1.3520	0.2522	1.5712	0.3278	1.7636	200
4	0.1578	1.2628	0.2515	1.4685	0.3698	1.7040	0.4780	1.9056	133
6	0.1765	1.2949	0.2788	1.5036	0.4087	1.7408	0.5265	1.9474	120
8	0.1857	1.3105	0.2925	1.5194	0.4278	1.7590	0.5505	1.9669	114
10	0.1913	1.3193	0.3006	1.5300	0.4392	1.7700	0.5648	1.9788	111
∞	0.2135	1.3555	0.3320	1.5719	0.4837	1.8152	0.6213	2.0236	100

θ_r	$m=1/3$		$m=1$		$m=2$		Pr_w
	$f''(0)$	$\theta'(0)$	$f''(0)$	$\theta'(0)$	$f''(0)$	$\theta'(0)$	
∞	0.7574	2.2314	1.2326	2.9863	1.7151	3.8128	100
	Hartree		Hartree				
−10	0.8241	2.7555	1.3368	3.0453	1.8561	3.8870	91
−8	0.8405	2.2864	1.3625	3.0601	1.8925	3.8963	89
−6	0.8678	2.3050	1.4050	3.0828	1.9500	3.9260	86
−4	0.9216	2.3342	1.4887	3.1265	2.0640	3.9811	80
−2	1.0784	2.4355	1.7306	3.2483	2.3922	4.1327	67
−1	1.3725	2.5957	2.1780	3.4514	2.9905	4.3906	50
−0.1	4.4521	3.6675	6.5168	4.7295	8.6382	5.9317	9
−0.01	10.2857	4.6266	15.2540	5.8716	20.4005	7.3291	1
−0.001	25.8312	5.4971	41.1722	6.9342	56.7603	8.6017	0.1
2	0.4033	1.9487	0.6675	2.6196	0.9360	3.3455	200
4	0.5852	2.1025	0.9597	2.8205	1.3401	3.5970	133
6	0.6436	2.1484	1.0526	2.8768	1.4680	3.6687	120
8	0.6725	2.1692	1.0983	2.9053	1.5308	3.7050	114
10	0.6897	2.1823	1.1255	2.9207	1.5682	3.7252	111
∞	0.7574	2.2314	1.2326	2.9863	1.7151	3.8128	100

m	−0.05	0	1/11	1/5	1/3	1	2
β	−0.105	0	1/6	1/3	1/2	1	4/3
	not physical	flat plate	wedge angle 30°	wedge angle 60°	wedge angle 90°	stagnation flow 180°	not physical

In the Falkner–Skan problem the flow is accelerated when $\beta > 0$ and retarded when $\beta < 0$. From the above table it is seen that our analysis concern mainly accelerated flows. We treated only one case of retarded flow ($m = -0.05$) which is not relevant to actual problems.

In Figs. 5 and 6 the wall heat transfer and the wall shear stress are shown as functions of the viscosity parameter θ_r. It is seen that, for negative values of θ_r, an increase of θ_r causes an increase in $\theta'(0)$ and $f''(0)$ and this increase becomes abrupt as θ_r approaches zero. When θ_r is positive, both $\theta'(0)$ and $f''(0)$ increase as θ_r increases. These figures also show that as the exponent m increases the wall heat transfer and the wall shear stress increase. In Fig. 7 the wall heat transfer is shown as function of the ambient Prandtl number. We see that $\theta'(0)$ increases as Pr_a increases for negative θ_r. The same happens for positive θ_r (not shown in the figure). In Fig. 8 the wall shear stress is shown as function of the ambient Prandtl number. It is seen that $f''(0)$ increases as Pr_a increases for negative θ_r. For positive θ_r (not shown in the figure) the wall shear stress decreases with Pr_a. As was expected, $f''(0)$ is independent from the Prandtl number when viscosity is constant. In Figs. 7 and 8, values for positive θ_r, have not been included in order to avoid confusion between many curves. Figs. 9 and 10 show the variation of $\theta'(0)$ and $f''(0)$ as functions of the exponent m. Both $\theta'(0)$ and $f''(0)$ increase as m increases.

In Figs. 11, 12 and 13 temperature profiles are shown for positive values of the viscosity parameter θ_r and ambient Prandtl numbers 1, 1000 and 10 000 whereas in Figs. 14, 15 and 16 temperature profiles are shown for negative values of θ_r and ambient Prandtl numbers 1, 1000 and 10 000. It is interesting to note that when $\theta_r < 0$ the temperature profiles lay below the constant viscosity profiles and when

Table 4
Values of $f''(0)$ and $\theta'(0)$ for $Pr_a = 1000$

θ_r	$m=-0.05$		$m=0$		$m=1/11$		$m=1/5$		Pr_w
	$f''(0)$	$\theta'(0)$	$f''(0)$	$\theta'(0)$	$f''(0)$	$\theta'(0)$	$f''(0)$	$\theta'(0)$	
∞	0.2135	2.8955	0.3320	3.3871	0.4837	3.9196	0.6213	4.3497	1000
			Hartree						
−10	0.2358	2.9675	0.3655	3.4183	0.5303	4.0090	0.6805	4.4544	909
−8	0.2414	2.9841	0.3737	3.4382	0.5419	4.0308	0.6952	4.4768	889
−6	0.2507	3.0122	0.3875	3.4674	0.5613	4.0674	0.7197	4.5193	857
−4	0.2693	3.0673	0.4149	3.5313	0.5998	4.1360	0.7684	4.5933	800
−2	0.3253	3.2228	0.4969	3.7025	0.7144	4.3288	0.9130	4.7951	667
−1	0.4384	3.4966	0.6598	4.0035	0.9395	4.6643	1.1960	5.1708	500
−0.1	2.4619	5.9127	3.2868	6.5642	4.2975	7.4044	5.2372	8.0871	91
−0.01	12.1937	9.9633	13.7116	10.5034	15.5545	11.2640	17.4622	11.9695	10
−0.001	19.5123	11.703	21.9213	12.2171	25.3048	12.9820	29.2519	13.8264	1
2	0.1045	2.4765	0.1668	2.8655	0.2465	3.3831	0.3187	3.7523	2000
4	0.1588	2.7010	0.2498	3.1184	0.3660	3.6735	0.4717	4.0668	1333
6	0.1770	2.7684	0.2774	3.1940	0.4054	3.7603	0.5219	4.1611	1200
8	0.1862	2.8014	0.2912	3.2329	0.4251	3.8030	0.5469	4.2230	1143
10	0.1917	2.8206	0.2995	3.2526	0.4368	3.8265	0.5619	4.2391	1111
∞	0.2135	2.8955	0.3320	3.3871	0.4837	3.9196	0.6213	4.3497	1000

θ_r	$m=1/3$		$m=1$		$m=2$		Pr_w
	$f''(0)$	$\theta'(0)$	$f''(0)$	$\theta'(0)$	$f''(0)$	$\theta'(0)$	
∞	0.7574	4.8320	1.2326	6.5291	1.7151	8.3622	1000
	Hartree		Hartree				
−10	0.8288	4.9346	1.3466	6.6460	1.8714	8.5750	909
−8	0.8466	4.9665	1.3749	6.6864	1.9101	8.6243	889
−6	0.8760	5.0086	1.4219	6.7427	1.9742	8.7732	857
−4	0.9347	5.0857	1.5153	6.8531	2.1043	8.8455	800
−2	1.1084	5.3231	1.7907	7.1514	2.4804	9.1238	667
−1	1.4464	5.7387	2.3219	7.6851	3.2024	9.7877	500
−0.1	6.1291	8.8911	9.2237	11.5740	12.3772	14.6776	91
−0.01	19.3483	12.8750	26.2086	16.1376	33.7091	20.0102	10
−0.001	33.2325	14.7135	48.4219	18.6522	64.7328	23.4420	1
2	0.3905	4.1812	0.6410	5.6666	0.8963	7.2111	2000
4	0.5762	4.5423	0.9415	6.1330	1.3130	7.8219	1333
6	0.6371	4.6412	1.0395	6.2645	1.4485	8.0029	1200
8	0.6674	4.6877	1.0881	6.3323	1.5157	8.0889	1143
10	0.6855	4.7178	1.1172	6.3677	1.5558	8.1367	1111
∞	0.7574	4.8320	1.2326	6.5291	1.7151	8.3622	1000

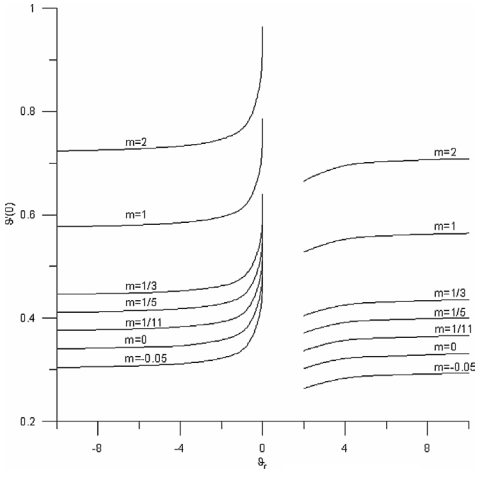

Fig. 5. Variation of wall heat transfer as function of viscosity parameter for different values of the exponent m and ambient Prandtl number 1.

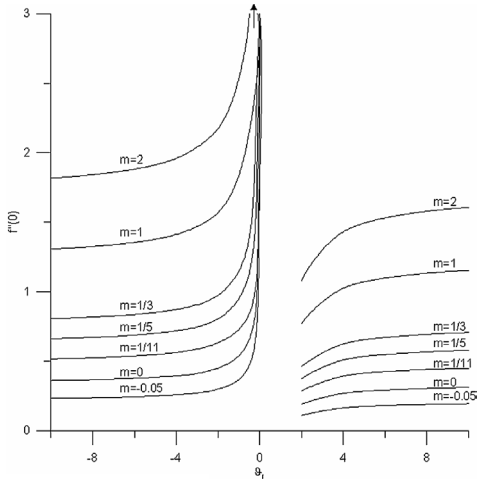

Fig. 6. Variation of wall shear stress as function of viscosity parameter for different values of the exponent m and ambient Prandtl number 1.

Table 5
Values of $f''(0)$ and $\theta'(0)$ for $Pr_a = 10\,000$

θ_r	$m=-0.05$		$m=0$		$m=1/11$		$m=1/5$		Pr_w
	$f''(0)$	$\theta'(0)$	$f''(0)$	$\theta'(0)$	$f''(0)$	$\theta'(0)$	$f''(0)$	$\theta'(0)$	
∞	0.2135	6.2122	0.3320	7.2974	0.4837	8.4917	0.6213	9.5107	10000
			Hartree						
−10	0.2354	6.3553	0.3649	7.4792	0.5315	8.6871	0.6821	9.7081	9091
−8	0.2409	6.3918	0.3730	7.5205	0.5434	8.7378	0.6972	9.7875	8889
−6	0.2500	6.4517	0.3871	7.5894	0.5631	8.8143	0.7224	9.8705	8571
−4	0.2682	6.5684	0.4146	7.7219	0.6026	8.9721	0.7727	10.0333	8000
−2	0.3232	6.8967	0.4971	8.0950	0.7209	9.4033	0.9228	10.4861	6667
−1	0.4336	7.4751	0.6621	8.7518	0.9554	10.1429	1.2208	11.2856	5000
−0.1	2.4945	12.7674	3.5412	14.6107	4.8973	16.7176	6.0974	18.4672	909
−0.01	19.6642	25.0785	23.6482	27.2765	28.5423	29.7023	32.8021	32.0000	99
−0.001	53.8275	34.6281	57.0817	36.3830	61.9973	38.3722	67.0011	40.7322	10
2	0.1057	5.3176	0.1663	6.2877	0.2439	7.3301	0.3144	8.2380	20000
4	0.1594	5.7948	0.2491	6.8375	0.3642	7.9642	0.4686	8.9261	13333
6	0.1775	5.9378	0.2767	7.0019	0.4042	8.1433	0.5197	9.1272	12000
8	0.1865	6.0069	0.2906	7.0833	0.4241	8.2350	0.5451	9.2477	11429
10	0.1919	6.0476	0.2987	7.1275	0.4361	8.2832	0.5604	9.2820	11111
∞	0.2135	6.2122	0.3320	7.2974	0.4837	8.4917	0.6213	9.5107	10000

θ_r	$m=1/3$		$m=1$		$m=2$		Pr_w
	$f''(0)$	$\theta'(0)$	$f''(0)$	$\theta'(0)$	$f''(0)$	$\theta'(0)$	
∞	0.7574	10.4846	1.2326	14.1583	1.7151	18.1850	10000
	Hartree		Hartree				
−10	0.8313	10.7259	1.3514	14.4672	1.8791	18.5725	9091
−8	0.8496	10.7921	1.3810	14.5254	1.9201	18.6325	8889
−6	0.8802	10.8877	1.4302	14.6667	1.9880	18.8256	8571
−4	0.9413	11.0731	1.5284	14.9245	2.1233	19.1708	8000
−2	1.1235	11.5843	1.8208	15.5920	2.5288	19.9810	6667
−1	1.4834	12.4869	2.3972	16.8000	3.3225	21.3033	5000
−0.1	7.1435	20.1259	11.3449	26.8043	15.4711	33.9245	909
−0.01	36.0405	34.1217	51.5265	44.0328	66.7306	54.8780	99
−0.001	71.9856	43.5017	93.6524	53.3058	118.4044	65.7657	10
2	0.3842	9.0487	0.6280	12.1714	0.8771	15.5111	20000
4	0.5719	9.8171	0.9325	13.2525	1.2996	16.8847	13333
6	0.6340	10.0521	1.0330	13.5378	1.4388	17.3002	12000
8	0.6649	10.1761	1.0831	13.6593	1.5081	17.4826	11429
10	0.6835	10.2538	1.1130	13.7366	1.5496	17.6073	11111
∞	0.7574	10.4846	1.2326	14.1583	1.7151	18.1850	10000

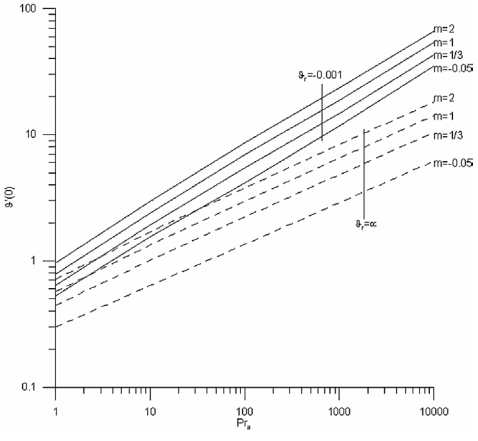

Fig. 7. Variation of wall heat transfer as function of the ambient Prandtl number for different values of the exponent m. Solid lines correspond to variable viscosity and dashed lines to constant viscosity.

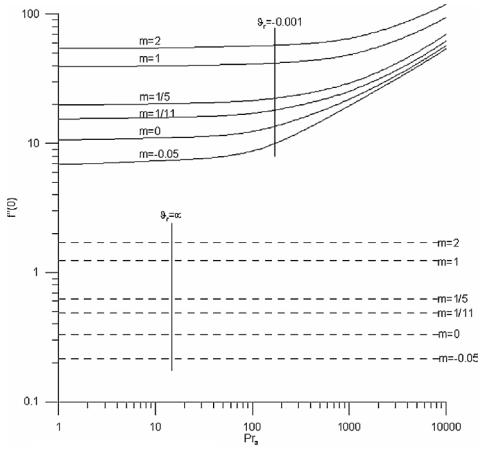

Fig. 8. Variation of wall shear stress as function of the ambient Prandtl number for different values of the exponent m. Solid lines correspond to variable viscosity and dashed lines to constant viscosity.

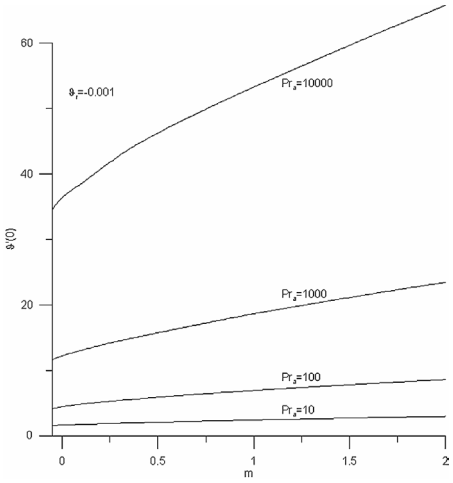

Fig. 9. Variation of wall heat transfer as function of the exponent m for different values of the ambient Prandtl number for $\theta_r = -0.001$.

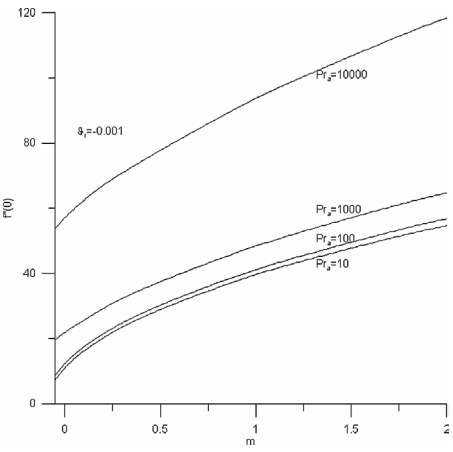

Fig. 10. Variation of wall shear stress as function of the exponent m for different values of the ambient Prandtl number for $\theta_r = -0.001$.

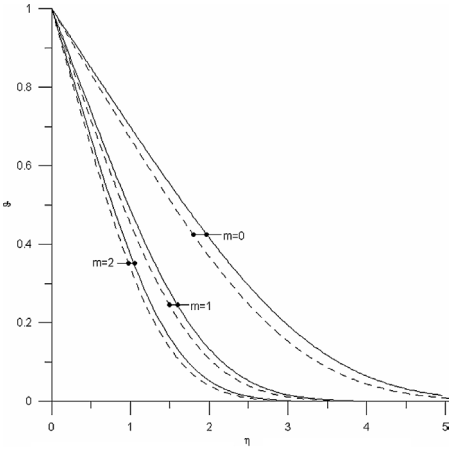

Fig. 11. Temperature distribution for ambient Prandtl number 1 and different values of the exponent m. Solid lines correspond to variable viscosity ($\theta_r = 2$) and dashed lines to constant viscosity ($\theta_r = \propto$).

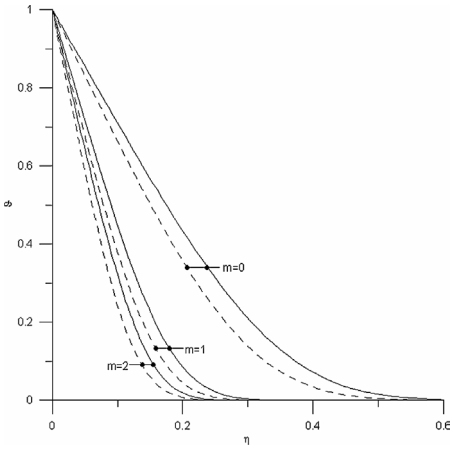

Fig. 12. Temperature distribution for ambient Prandtl number 1000 and different values of the exponent m. Solid lines correspond to variable viscosity ($\theta_r = 2$) and dashed lines to constant viscosity ($\theta_r = \propto$).

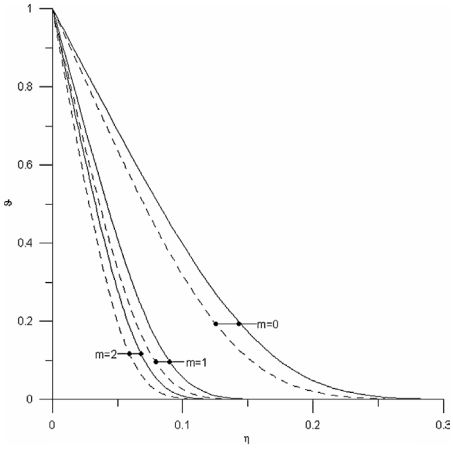

Fig. 13. Temperature distribution for ambient Prandtl number 10 000 and different values of the exponent m. Solid lines correspond to variable viscosity ($\theta_r = 2$) and dashed lines to constant viscosity ($\theta_r = \propto$).

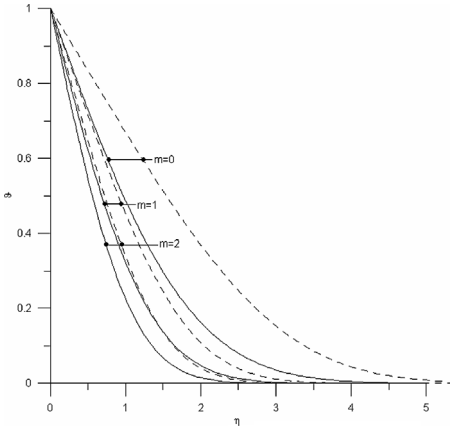

Fig. 14. Temperature distribution for ambient Prandtl number 1 and different values of the exponent m. Solid lines correspond to variable viscosity ($\theta_r = -0.001$) and dashed lines to constant viscosity ($\theta_r = \propto$).

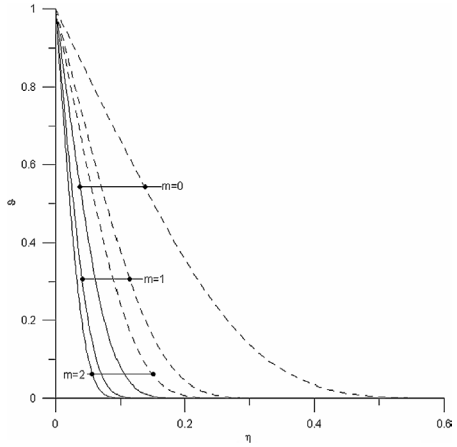

Fig. 15. Temperature distribution for ambient Prandtl number 1000 and different values of the exponent m. Solid lines correspond to variable viscosity ($\theta_r = -0.001$) and dashed lines to constant viscosity ($\theta_r = \infty$).

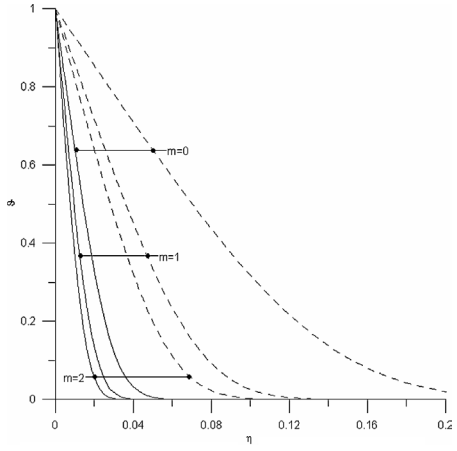

Fig. 16. Temperature distribution for ambient Prandtl number 10 000 and different values of the exponent m. Solid lines correspond to variable viscosity ($\theta_r = -0.001$) and dashed lines to constant viscosity ($\theta_r = \infty$).

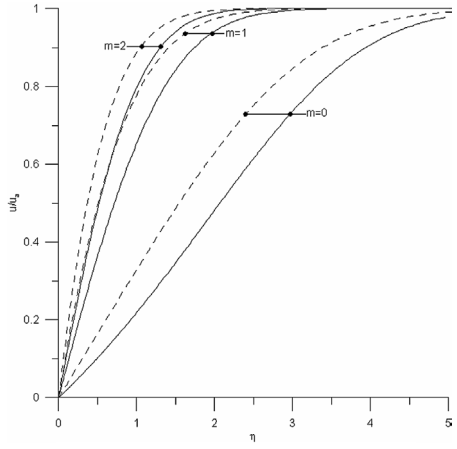

Fig. 17. Velocity distribution for ambient Prandtl number 1 and different values of the exponent m. Solid lines correspond to variable viscosity ($\theta_r = 2$) and dashed lines to constant viscosity ($\theta_r = \infty$).

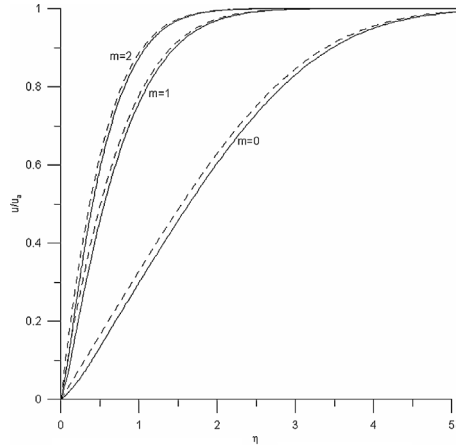

Fig. 18. Velocity distribution for ambient Prandtl number 1000 and different values of the exponent m. Solid lines correspond to variable viscosity ($\theta_r = 2$) and dashed lines to constant viscosity ($\theta_r = \infty$).

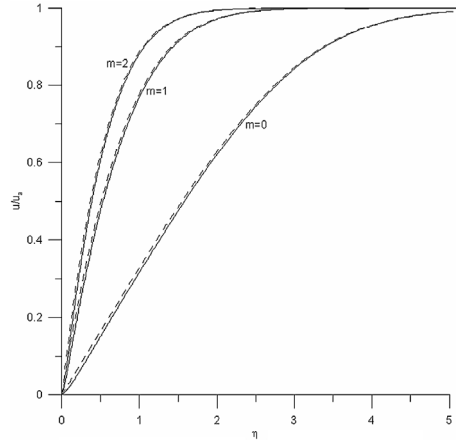

Fig. 19. Velocity distribution for ambient Prandtl number 10 000 and different values of the exponent m. Solid lines correspond to variable viscosity ($\theta_r = 2$) and dashed lines to constant viscosity ($\theta_r = \infty$).

$\theta_r > 0$ the temperature profiles lay above the constant viscosity profiles. It is also seen that as the ambient Prandtl number increases the temperature profiles become "narrower" (the width of temperature profile decreases). The exponent m has the same influence, that is, as m increases the temperature profile width decreases. Figs. 17, 18 and 19 show the corresponding velocity profiles for positive θ_r and Figs. 20, 21 and 22 show the corresponding velocity profiles for negative θ_r. We see that when $\theta_r < 0$ the velocity profiles lay above the constant viscosity Profiles and the opposite happens when $\theta_r > 0$. The explanation is the following: from the above tables we see that for negative values of θ_r the Prandtl number at the plate (Pr_w) is smaller than the ambient one and for positive values of θ_r the Pr_w is greater than the ambient one. Obviously the same happens with viscosity taking into account that thermal diffusivity is constant. This means that viscosity decreases inside the boundary layer for $\theta_r < 0$ and increases for $\theta_r > 0$. It is well known in fluid mechanics that when viscosity decreases the velocity increases

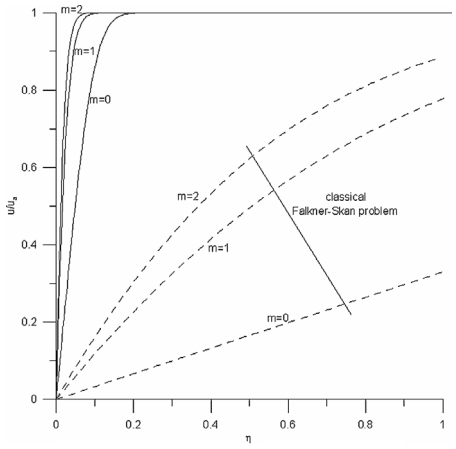

Fig. 20. Velocity distribution for ambient Prandtl number 1 and different values of the exponent m. Solid lines correspond to variable viscosity ($\theta_r = -0.001$) and dashed lines to constant viscosity ($\theta_r = \infty$).

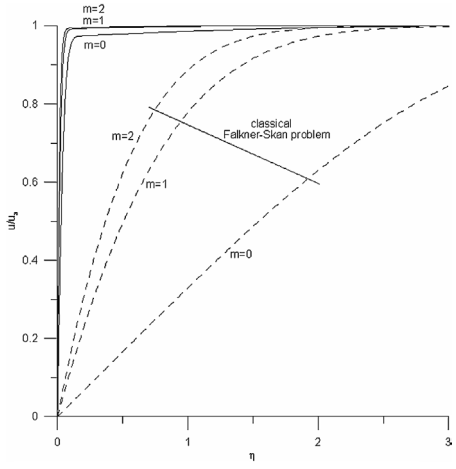

Fig. 21. Velocity distribution for ambient Prandtl number 1000 and different values of the exponent m. Solid lines correspond to variable viscosity ($\theta_r = -0.001$) and dashed lines to constant viscosity ($\theta_r = \infty$).

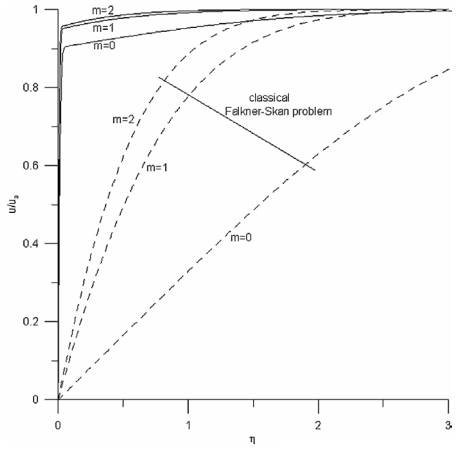

Fig. 22. Velocity distribution for ambient Prandtl number 10 000 and different values of the exponent m. Solid lines correspond to variable viscosity ($\theta_r = -0.001$) and dashed lines to constant viscosity ($\theta_r = \infty$).

(the fluid flows easier) and vice versa. For that reason the velocity profiles in Figs. 20, 21 and 22 lay above the constant viscosity profiles and below them in Figs. 17, 18 and 19. The increased velocities in Figs. 20, 21 and 22 ($\theta_r < 0$) suppress the corresponding temperature profiles in Figs. 14, 15 and 16 and for that reason these profiles lay below the constant viscosity profiles. The opposite happens in Figs. 11, 12 and 13.

It should be mentioned here that all the constant viscosity profiles (dashed lines) in the above figures have been produced by the present method and are identical with those produced by the classical similarity method with constant viscosity (velocity similarity profiles with constant viscosity are given on page 245 in White [14] and on page 151 in Schlichting [19]).

4. Conclusions

The foregoing results are the first complete calculations of the effect of variable viscosity on the classical Falkner–Skan flow and can be summarized as follows:

1. The wall heat transfer $\theta'(0)$ and the wall shear stress $f''(0)$ increase as the viscosity parameter θ_r increases. The increase becomes abrupt as θ_r approaches zero.
2. The wall heat transfer $\theta'(0)$ increases as Pr_a increases for both positive and negative values of θ_r.
3. The wall shear stress $f''(0)$ increases as Pr_a increases for $\theta_r < 0$ and decreases for $\theta_r > 0$.
4. The wall heat transfer $\theta'(0)$ and the wall shear stress $f''(0)$ increase as the exponent m increases.
5. The temperature profiles lay below the constant viscosity profiles when $\theta_r < 0$ and above them when $\theta_r > 0$.
6. The velocity profiles lay above the constant viscosity profiles when $\theta_r < 0$ and below them when $\theta_r > 0$.

References

[1] V.M. Falkner, S.W. Skan, Some approximate solutions of the boundary layer equations, Philos. Mag. 12 (1931) 865–896.
[2] D.R. Hartree, On an equation occurring in Falkner and Skan's approximate treatment of the equations of the boundary layer, Part II, Proc. Cambridge Philos. Soc. 33 (1937) 223–239.
[3] A. Bejan, Convection Heat Transfer, John Wiley, New York, 1995.
[4] E.R.G. Eckert, Die Berechnung des Warmeuberganges in der Laminaren Grenzschicht um stromter Korper, VDI-Forschungsheft 416 (1942) 1–24.
[5] H.-T. Lin, L.-K. Lin, Similarity solutions for laminar forced convection heat transfer from wedges to fluids of any Prandtl number, Int. J. Heat Mass Transfer 30 (1987) 1111–1118.
[6] H. Herwig, G. Wickern, The effect of variable properties on laminar boundary layer flow, Warme und Stoffubertragung 20 (1986) 47–57.
[7] M.A. Hossain, M.Z. Munir, M.S. Hafiz, H.S. Takhar, Flow of viscous incompressible fluid with temperature dependent viscosity past a permeable wedge with uniform surface heat flux, Heat Mass Transfer 36 (2000) 333–341.

[8] Md.A. Hossain, Md.S. Munir, D.A.S. Rees, Flow of viscous incompressible fluid with temperature dependent viscosity and thermal conductivity past a permeable wedge with uniform surface heat flux, Int. J. Thermal Sci. 39 (2000) 635–644.
[9] E.M.A. Elbashbeshy, M.F. Dimian, Effect of radiation on the flow and heat transfer over a wedge with variable viscosity, Appl. Math. Comput. 132 (2002) 445–454.
[10] K. Nanbu, Unsteady Falkner–Skan flow, J. Appl. Math. Phys. (ZAMP) 22 (1971) 1167–1172.
[11] J.X. Ling, A. Dybbs, Forced convection over a flat plate submerged in a porous medium: variable viscosity case, ASME, Paper 87-WA/HT-23, New York, 1987.
[12] S.V. Patankar, Numerical Heat Transfer and Fluid Flow, McGraw-Hill, New York, 1980.
[13] S.V. Patankar, D.B. Spalding, Heat and Mass Transfer in Boundary Layers, Intertext, London, 1970.
[14] F. White, Viscous Fluid Flow, McGraw-Hill, New York, 1991.
[15] A. Pantokratoras, Laminar free-convection over a vertical isothermal plate with uniform blowing or suction in water with variable physical properties, Int. J. Heat Mass Transfer 45 (2002) 963–977.
[16] I. Pop, R.S.R. Gorla, M. Rashidi, The effect of variable viscosity on flow and heat transfer to a continuous moving flat plate, Int. J. Engrg. Sci. 30 (1992) 1–6.
[17] A. Pantokratoras, Further results on the variable viscosity on flow and heat transfer to a continuous moving flat plate, Int. J. Engrg. Sci. 42 (2004) 1891–1896.
[18] S. Harris, D. Ingham, I. Pop, Unsteady heat transfer in impulsive Falkner–Skan flows: constant wall temperature case, Eur. J. Mech. B Fluids 21 (2002) 447–468.
[19] H. Schlichting, Boundary-Layer Theory, McGraw-Hill, New York, 1968.